

We have presented the graphical abstract image and text for your article below. This briefly summarises your work, and will be presented with your article online.

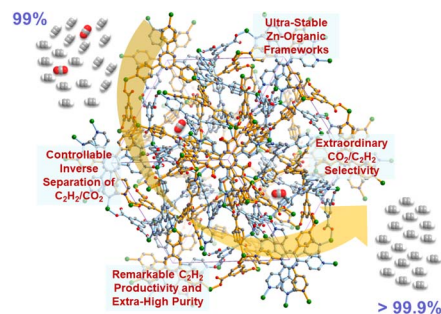
PAPER

1

Controllable inverse C_2H_2/CO_2 separation in ultra-stable Zn-organic frameworks for efficient removal of trace CO_2 from acetylene

Jia Yu, Jing Zhang, Peng Zhang,* Ying Wang, Shu-Ni Li and Quan-Guo Zhai*

- 4 Ultra-stable Zn-organic frameworks with controllable inverse adsorption separation of C_2H_2/CO_2 demonstrate extraordinary CO_2 -preferred selectivity and a remarkable productivity of C_2H_2 with an extra-high purity of more than 99.9% from the CO_2/C_2H_2 (1/99) mixture²²²² (1/99) mixture.



Please check this proof carefully. Our staff will not read it in detail after you have returned it.

Please send your corrections either as a copy of the proof PDF with electronic notes attached or as a list of corrections. **Do not edit the text within the PDF or send a revised manuscript** as we will not be able to apply your corrections. Corrections at this stage should be minor and not involve extensive changes.

Proof corrections must be returned as a single set of corrections, approved by all co-authors. No further corrections can be made after you have submitted your proof corrections as we will publish your article online as soon as possible after they are received.

Please ensure that:

- The spelling and format of all author names and affiliations are checked carefully. You can check how we have identified the authors' first and last names in the researcher information table on the next page. **Names will be indexed and cited as shown on the proof, so these must be correct.**
- Any funding bodies have been acknowledged appropriately and included both in the paper and in the funder information table on the next page.
- All of the editor's queries are answered.
- Any necessary attachments, such as updated images or ESI files, are provided.

Translation errors can occur during conversion to typesetting systems so you need to read the whole proof. In particular please check tables, equations, numerical data, figures and graphics, and references carefully.

Please return your **final** corrections, where possible within **48 hours** of receipt following the instructions in the proof notification email. If you require more time, please notify us by email to materialsA@rsc.org.

Funding information

Providing accurate funding information will enable us to help you comply with your funders' reporting mandates. Clear acknowledgement of funder support is an important consideration in funding evaluation and can increase your chances of securing funding in the future.

We work closely with Crossref to make your research discoverable through the Funding Data search tool (<http://search.crossref.org/funding>). Funding Data provides a reliable way to track the impact of the work that funders support. Accurate funder information will also help us (i) identify articles that are mandated to be deposited in **PubMed Central (PMC)** and deposit these on your behalf, and (ii) identify articles funded as part of the **CHORUS** initiative and display the Accepted Manuscript on our web site after an embargo period of 12 months.

Further information can be found on our webpage (<http://rsc.li/funding-info>).

What we do with funding information

We have combined the information you gave us on submission with the information in your acknowledgements. This will help ensure the funding information is as complete as possible and matches funders listed in the Crossref Funder Registry.

If a funding organisation you included in your acknowledgements or on submission of your article is not currently listed in the registry it will not appear in the table on this page. We can only deposit data if funders are already listed in the Crossref Funder Registry, but we will pass all funding information on to Crossref so that additional funders can be included in future.

Please check your funding information

The table below contains the information we will share with Crossref so that your article can be found *via* the Funding Data search tool. **Please check that the funder names and grant numbers in the table are correct and indicate if any changes are necessary to the Acknowledgements text.**

Funder name	Funder's main country of origin	Funder ID (for RSC use only)	Award/grant number
Natural Science Foundation of Shaanxi Province	China	501100007128	2021JLM-20
National Natural Science Foundation of China	China	501100001809	22071140
Fundamental Research Funds for the Central Universities	China	501100012226	GK202101002

Researcher information

Please check that the researcher information in the table below is correct, including the spelling and formatting of all author names, and that the authors' first, middle and last names have been correctly identified. **Names will be indexed and cited as shown on the proof, so these must be correct.**

If any authors have ORCID or ResearcherID details that are not listed below, please provide these with your proof corrections. Please ensure that the ORCID and ResearcherID details listed below have been assigned to the correct author. Authors should have their own unique ORCID iD and should not use another researcher's, as errors will delay publication.

Please also update your account on our online [manuscript submission system](#) to add your ORCID details, which will then be automatically included in all future submissions. See [here](#) for step-by-step instructions and more information on author identifiers.

First (given) and middle name(s)	Last (family) name(s)	ResearcherID	ORCID iD
Jia	Yu		
Jing	Zhang		

Peng	Zhang		
Ying	Wang		
Shu-Ni	Li		0000-0002-6614-9241
Quan-Guo	Zhai		0000-0003-1117-4017

Queries for the attention of the authors

Journal: **Journal of Materials Chemistry A**








Paper: **d2ta07473g**

Title: **Controllable inverse C₂H₂/CO₂ separation in ultra-stable Zn-organic frameworks for efficient removal of trace CO₂ from acetylene**

For your information: You can cite this article before you receive notification of the page numbers by using the following format: (authors), J. Mater. Chem. A, (year), DOI: 10.1039/d2ta07473g.

Editor's queries are marked on your proof like this **1**, **2**, etc. and for your convenience line numbers are indicated like this 5, 10, 15, ...

Please ensure that all queries are answered when returning your proof corrections so that publication of your article is not delayed.

Query Reference	Query	Remarks
1	<p>We have shown the changes (if any) made by the copyeditor in your proof as part of a trial. You can view these as edits in the Proof Central interface. Did you find this useful? Please also consider completing this short three-minute survey to give more detailed feedback: https://www.smartsurvey.co.uk/s/TAttrackchanges/.</p> <p>Please tick this box if you find this useful. <input type="checkbox"/></p>	
2	<p>Please check that the inserted CCDC numbers are correct.</p>	
3	<p>Have all of the author names been spelled and formatted correctly? Names will be indexed and cited as shown on the proof, so these must be correct. No late corrections can be made.</p> <p>Please tick this box or indicate your confirmation if you have no corrections to make to the proof <input type="checkbox"/></p>	
4	<p>The sentence beginning "Ultra-stable Zn-organic frameworks with controllable inverse..." has been altered for clarity, please check that the meaning is correct</p>	
5	<p>The sentence beginning "In general, there are two kinds of C₂H₂ purification..." has been altered for clarity, please check that the meaning is correct</p>	
6	<p>The sentence beginning "To date, most of the MOF-based purification..." has been altered for clarity, please check that the meaning is correct</p>	
7	<p>The sentence beginning "However, a high-valence metal centre..." has been altered for clarity, please check that the meaning is correct</p>	
8	<p>The sentence beginning "After the adsorption and separation..." has been altered for clarity, please check that the meaning is correct</p>	

9

Have all of the funders of your work been fully and accurately acknowledged?

Please tick this box or indicate your confirmation if you have no corrections to make to the proof

PAPER

Controllable inverse C₂H₂/CO₂ separation in ultra-stable Zn-organic frameworks for efficient removal of trace CO₂ from acetylene†Jia Yu, Jing Zhang, Peng Zhang,* Ying Wang, Shu-Ni Li  and Quan-Guo Zhai *

Cite this: DOI: 10.1039/d2ta07473g

It is of great challenge to produce highly pure C₂H₂ from the CO₂/C₂H₂ mixture because of their similar physical properties. Metal-organic frameworks (MOFs) have shown great potential in purifying C₂H₂ by virtue of their versatile pore environment with excellent tunability. However, the rational exploration of ideal MOF adsorbents with CO₂-preferred CO₂/C₂H₂ separation performance (also called inverse C₂H₂/CO₂ separation) is extremely difficult. In this work, we demonstrate a new Zn-MOF family (SNNU-334–336) with special CO₂-preferred CO₂/C₂H₂ separation performance, which can be rationally controlled by functional groups as well as temperature. Notably, SNNU-334–336 MOFs show extremely high stability, and SNNU-336 can maintain a stable structure even after 7 days in boiling water and 30 days in air, which is unprecedented for all Zn-based MOF materials. Different to common MOF adsorbents, the adsorption isotherms of SNNU-334–336 MOFs for C₂H₂ and CO₂ under the same temperature all have an intersection point (we called the inverse point), which gradually moves to the high-pressure region with the increase of temperature and changes with the pore environment variation. So, SNNU-334–336 MOFs can be rationally controlled from C₂H₂-selective to CO₂-selective CO₂/C₂H₂ adsorption separation adsorbents. IAST selectivity calculation indicates that a very high CO₂ over C₂H₂ selectivity (3595.4) can be achieved, which nearly surpasses those of all reported MOFs with CO₂-preferred CO₂/C₂H₂ separation performance. Fixed-bed column breakthrough experiments further prove that SNNU-334–336 MOFs all have controllable inverse CO₂/C₂H₂ separation ability and can produce C₂H₂ with extra-high purity (>99.9%) from the CO₂/C₂H₂ (1/99) mixture.

Received 23rd September 2022
Accepted 24th October 2022

DOI: 10.1039/d2ta07473g

rsc.li/materials-a**Introduction**

Acetylene, C₂H₂, as an important fuel gas and industrial product, has been widely used in the production of various basic petrochemical products, such as butanediol, acrylic acid and acetylene alcohol.^{1,2} It is usually prepared by hydrocarbon cracking or combustion of natural gas in industry, and thus the CO₂ impurity (*ca.* 3.2–3.5%) is introduced inevitably^{3–6} which further limits its direct applications. At present, cryogenic distillation or the solvent extraction technique is used to purify acetylene. However, this leads to serious energy loss, environmental pollution and other problems, and the purity cannot still meet the requirement of applications.⁷ Therefore, it is necessary to develop more promising CO₂-selective adsorbent-based separation techniques to obtain high-purity C₂H₂.

Key Laboratory of Macromolecular Science of Shaanxi Province, School of Chemistry & Chemical Engineering, Shaanxi Normal University, Xi'an, Shaanxi, 710062, China.
E-mail: peng.zhang@snnu.edu.cn; zhaiqg@snnu.edu.cn

† Electronic supplementary information (ESI) available: Single crystal data, additional crystal structures, PXRD patterns, gas adsorption isotherms, IAST selectivity data, and GCMC simulation results. CCDC 2209077–2209079. For ESI and crystallographic data in CIF or other electronic format see DOI: <https://doi.org/10.1039/d2ta07473g>

Nevertheless, it is a difficult task to obtain CO₂-selective adsorbents as a result of the similar molecular sizes (C₂H₂: 3.3 × 3.3 × 5.7 Å³, CO₂: 3.2 × 3.3 × 5.4 Å³)^{8–10} and physicochemical properties of CO₂ and C₂H₂.^{11,12}

Metal-organic frameworks (MOFs) formed by self-assembly of metal ions and organic ligands *via* coordination bonds^{13–16} are known for their highly adjustable pore sizes and surface environment,^{17–20} and have shown great potential in CO₂/C₂H₂ separation.^{21–23} In general, there are two kinds of C₂H₂ purification methods based on MOFs₂ purification, *i.e.* purification using C₂H₂-selective MOFs and purification using CO₂-selective MOFs.² To date, most of the MOF-based purification methods belong to the former category owing to the fact that the electronic structure of C₂H₂ molecules is more liable to interact with MOF active sites compared with CO₂.^{24–26} However, it requires adsorption and subsequent desorption processes to purify C₂H₂ using the former method, and thus it seems to have low-efficiency. By contrast, high-purity C₂H₂ is expected to be directly obtained using the latter method where CO₂ is removed *via* preferential adsorption by MOFs, that is, so-called inverse C₂H₂/CO₂ separation.^{27–29} Until now, limited MOFs with C₂H₂/CO₂ inverse separation properties have been reported such as Mn(bdc)(dpe),³⁰ Ce^{IV}-MIL-140-4F,³¹ MUF-16 family,³² CD-MOF-1,

CD-MOF-2,³³ Tm-MOF,³⁴ and $[\text{Zn}(\text{atz})(\text{BDC}-\text{Cl}_4)_{0.5}]_n$.³⁵ However, the temperature or pressure dependent behaviour of reversal $\text{C}_2\text{H}_2/\text{CO}_2$ adsorption and separation processes has not been explored in currently developed MOFs. Undoubtedly, it requires elaborate design of the pore environment of MOF materials for controllable $\text{C}_2\text{H}_2/\text{CO}_2$ inverse adsorption performance.

In addition, the poor stability of MOFs especially in water or air seriously limits their large-scale application in industry.^{36,37} It has been demonstrated that high stability could be achieved by introducing mixed metal ions into MOF materials.³⁰ However, it results in more difficulty in synthesis due to the simultaneous introduction of two or more kinds of metal ions and in predicting the structural motif. It is highly expected to obtain stable MOF materials containing single metal ions. In fact, few examples have shown satisfactory water stability, such as ZIF-8 (ref. 38) and UiO-66.³⁹ However, a high-valence metal centre and high coordination number are necessary in those MOFs, thus limiting the synthesis method to a few metal elements in the periodic table. Therefore, developing new universal synthesis methodologies is crucial for pushing them to practical applications.

Here, we synthesized three new Zn-MOFs, SNNU-334–336, which not only exhibit ultra-stable structures but achieve controllable $\text{C}_2\text{H}_2/\text{CO}_2$ inverse separation *via* temperature change. Specifically, SNNU-336 maintains a stable structure even after 7 days in boiling water and 30 days in air, which is unprecedented for all Zn-based MOF materials and even comparable to that of famous UiO-66 materials. By adjusting the ultra-microporous environment with functional groups, these Zn-MOF adsorbents can successfully remove trace CO_2 impurities from $\text{CO}_2/\text{C}_2\text{H}_2$ mixtures and directly produce high purity C_2H_2 (the purity can reach more than 99.9%). The irregular cages with a pore size of about 6 Å in these Zn-MOFs are the main contributor to $\text{CO}_2/\text{C}_2\text{H}_2$ storage and separation. The change of reverse points from low to high pressure proved that the inverse adsorption performance of SNNU-334–336 could be rationally controlled by temperature. Dynamic breakthrough experiments further support our speculation about the properties of SNNU-334–336. Overall, the excellent properties of the MOF materials, *i.e.*, high moisture, acid, and alkali stability and high CO_2 selectivity indicate that SNNU-334–336 materials have great potential in industrial production of high-purity C_2H_2 .

Experimental section

Materials

$\text{Zn}(\text{NO}_3)_2 \cdot 6\text{H}_2\text{O}$, 1,3,5-benzenetricarboxylic acid (BTC), 4-amino-1,3,5-benzenetricarboxylic acid (NH_2 -BTC), 2,4,6-tri(4-pyridinyl)-1-pyridine (TPP), 1,3,5-tris(4-pyridyl)benzene (TPB), *N,N*-dimethylformide (DMF), and ethanol (EtOH) were purchased from China National Pharmaceutical Group Corporation (Shanghai, China).

Synthesis of SNNU-334

$\text{Zn}(\text{NO}_3)_2 \cdot 6\text{H}_2\text{O}$ (60 mg, 0.2 mmol), BTC (21 mg, 0.1 mmol), and TPP (15 mg, 0.05 mmol) were added to 6 ml of a mixed solvent of

DMF/EtOH/ H_2O ($V/V/V = 2/2/2$) in a 20 mL glass vial, and ultrasonication was performed for 3 h. After being sealed, the solution was heated to 100 °C for 3 days to obtain light yellow octahedral crystals. The crystals were washed with DMF and dried under a nitrogen atmosphere. The yield was about 65% on the basis of metal salts.

Synthesis of SNNU-335

$\text{Zn}(\text{NO}_3)_2 \cdot 6\text{H}_2\text{O}$ (60 mg, 0.2 mmol), NH_2 -BTC (11 mg, 0.05 mmol), and TPB (15 mg, 0.05 mmol) were added to 6 mL of a mixed solvent of DMF/EtOH/ H_2O ($V/V/V = 2/2/2$) in a 20 mL glass vial, and ultrasonication was performed for 3 h. After being sealed, the solution was heated to 100 °C for 3 days to obtain colorless octahedral crystals. The crystals were washed with DMF and dried under a nitrogen atmosphere. The yield was about 68% on the basis of metal salts.

Synthesis of SNNU-336

$\text{Zn}(\text{NO}_3)_2 \cdot 6\text{H}_2\text{O}$ (60 mg, 0.2 mmol), BTC (21 mg, 0.1 mmol), and TPB (15 mg, 0.05 mmol) were added to 6 ml of a mixed solvent of DMF/EtOH/ H_2O ($V/V/V = 2/2/2$) in a 20 mL glass vial, and ultrasonication was performed for 3 h. After being sealed, the solution was heated to 100 °C for 3 days to obtain yellow octahedral crystals. The crystals were washed with DMF and dried in a nitrogen atmosphere. The yield was about 68% on the basis of metal salts.

Structural characterization

The powder X-ray diffraction (PXRD) tests were carried out on a MiniFlex 600 X-ray diffractometer (Rigaku, Japan). Thermogravimetric analyses (TGA) were carried out on a NETSCHZ STA-449C thermal analyzer with a ramp rate of 5 °C min^{-1} in a nitrogen atmosphere. Crystallographic data of SNNU-334–336 were obtained on a Bruker APEX II diffractometer with graphite-monochromated Mo $\text{K}\alpha$ radiation and analyzed with SHELXTL and Olex 2 software.^{40–42} All non-hydrogen atoms were refined isotropically. The detailed crystallographic data and the structure refinement parameters of SNNU-334–336 are summarized in Tables S1 and S2.†

Gas adsorption experiments

Gas adsorption isotherms were obtained on a Micromeritics ASAP 2020 HD88 Surface-area and Pore-size Analyzer. All the gases used in the adsorption experiments were of 99.99% purity. Dynamic breakthrough experiments were carried out on a home-made device with a temperature of 263 K to 298 K being controlled by a circulating water bath. After the adsorption and separation in the through-column unit adsorption bed, the gas was then flowed into the gas chromatographic detection system for detection and analysis.

In order to evaluate the permanent porosities of SNNU-334–336, CO_2 adsorption measurements were conducted at 195 K. Gas adsorption measurements of SNNU-334–336 for single-component C_2H_2 and CO_2 were performed at 263–308 K. The MOF sample was soaked in methanol for 3 days and exchanged

every 8 h, and the solvent molecules in the pores were completely removed at 60 °C in a vacuum for 24 h. The separation ability of SNNU-334–336 for CO₂/C₂H₂ was calculated by ideal adsorbed solution theory (IAST). To further verify the practical separation ability of these three MOFs for C₂H₂ purification, breakthrough column experiments were carried out. Activated SNNU-334–336 crystalline powder samples (SNNU-334: 730.5 mg; SNNU-335: 546.3 mg; SNNU-336: 780.0 mg) were filled in a stainless-steel column as the adsorbent bed. The samples were purged with helium gas for 12 h at room temperature to be further activated. Subsequently, mixed gases with different components (such as 50/50, 99/1) were introduced into the column. Before any new testing, a helium flow of 20 mL min⁻¹ had to be maintained for at least 5 h to remove the residual gas molecules in the column.

Results and discussion

Crystal structures of SNNU-334–336

Since SNNU-334–336 MOFs are isostructural, only the crystal structure of SNNU-334 is described in detail herein. The single-crystal X-ray diffraction data reveal that SNNU-334 crystallizes in the cubic *Pa3* space group. The asymmetric coordination unit is composed of one Zn atom ion, two BTC ligands and two TPP ligands (Fig. 1). Each Zn ion is four-coordinated with two O atoms from two BTC ligands and two N atoms from two TPP ligands. Each TPP ligand connects three Zn atoms through three pyridine N sites. Also, each BTC linker connects three Zn atoms through three O sites from three carboxylate groups. The extension of such a simple linkage between metal centers and organic linkers generates a 3D metal–organic architecture (Fig. 1 and S1†). Clearly, BTC, TPP and the Zn atom can be

viewed as 3-, 3- and 4-connected nodes, which were connected to form a new (3,4)-connected topological net with a point symbol of {8³}₄{8⁶}₃.

On the other hand, four types of trigonal prismatic metal–organic cages are observed (Fig. 1c). Each cage contains six Zn atoms located on the six vertices of the triangular prism. Besides Zn ions, one BTC and four TPP, three BTC and two TPP, two BTC and three TPP, and four BTC and one TPP exist in Cages A–D with a diameter of about 6 Å, 4 Å, 5 Å and 4 Å, respectively. With Cage A as the centre, the other three kinds of smaller cages were connected by sharing TPP ligands and stacked around each Cage A to form the final cage–cage stacking structure of SNNU-334 (Fig. 1b). The central pyridyl-N atoms of TPP ligands located on the surface of cages act as Lewis basic sites, which may enhance the affinity between gas molecules and the MOF framework. The same structure is found in SNNU-336 with the TPP ligands of SNNU-334 substituted by TPB ligands. Different from SNNU-336, the BTC ligand in SNNU-335 is further functionalized by –NH₂ groups.

Finally, SNNU-334–336 MOFs exhibit a typical double interpenetrating structure. With two parts interpenetrating each other from opposite directions (Fig. 1d–f), four types of metal–organic cages still exist after the interpenetration. Such 2-fold interpenetration effectively improves the stability of these three MOFs, which is critical for the practical applications of gas adsorbents.

MOF stability

The phase purity and stability of SNNU-334–336 were confirmed by the powder X-ray diffraction (PXRD) and thermogravimetric analysis (TGA). It can be observed from the TG curves (Fig. 2) that the three MOFs all can remain stable in the range of 50–

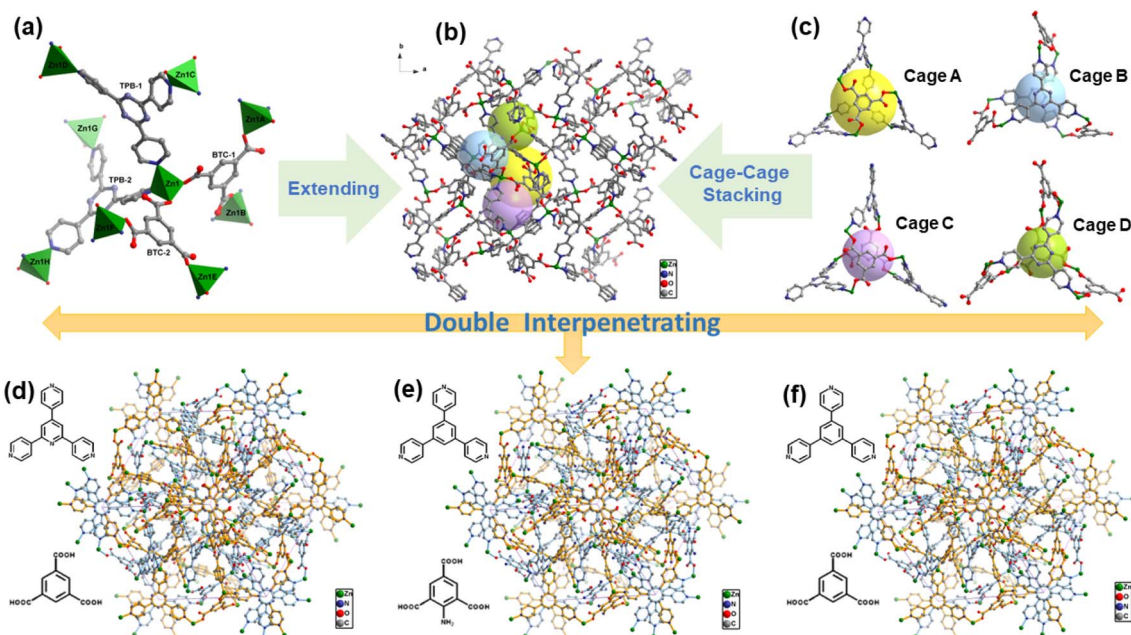


Fig. 1 (a) The basic coordination environment and linkage for Zn atoms and organic ligands; (b) the 3D metal–organic coordination framework; (c) four different metal–organic cages; (d–f) the whole 2-fold interpenetrated architectures with different functional groups for SNNU-334–336.

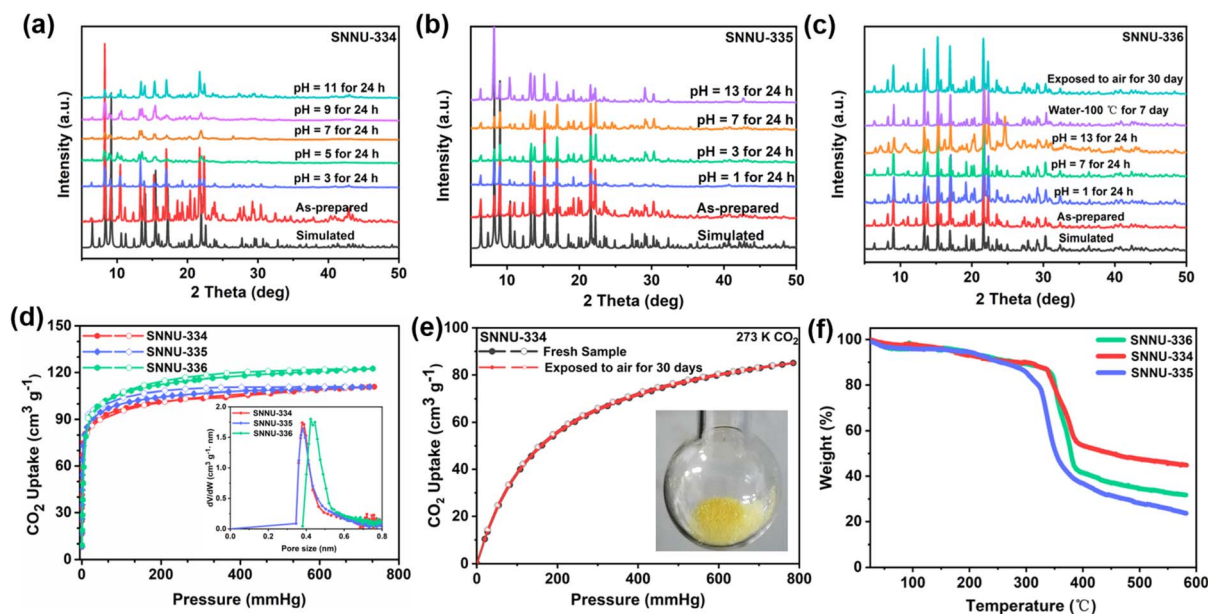


Fig. 2 The PXRD patterns of (a) SNNU-334; (b) SNNU-335 and (c) SNNU-336 treated under different conditions; (d) the CO₂ adsorption curves at 195 K and the pore size distributions; (e) the CO₂ adsorption curves of the fresh SNNU-334 sample and after exposure to air for 30 days (inset picture); (f) TGA curves of SNNU-334-336.

300 °C and the weight losses are about 20%, which could be attributed to the loss of solvent molecules trapped in the skeleton. The chemical stability of MOF adsorbents plays an important role in the gas adsorption and separation applications. It is noted that most of the Zn-MOFs are vulnerable to structural damage in water and even in the atmospheric environment due to the relatively weak coordination bonding between Zn ions and donors. But the PXRD results showed that the crystallinity of SNNU-336 did not change and its structure remained intact (Fig. 2c) even after being exposed in air for 30 days and soaking in water at 100 °C for 7 days. SNNU-336 was further immersed in solutions of pH = 1–13 to investigate the acid and alkaline resistance. After 24 h, the MOF skeleton remained stable according to PXRD results. SNNU-334 and SNNU-335 were subjected to the same experiments with similar results (Fig. 2 and S2†). In addition, the CO₂ adsorption performance of SNNU-334 exposed to air for 30 days was tested, which completely coincided with the adsorption curves of the fresh MOF samples (Fig. 2e), further confirming the moisture stability of the samples in air. To the best of our knowledge, SNNU-334–336 MOFs are comparable to Zn-MOFs exhibiting such an ultra-high physical and chemical stability. In our opinion, the four-coordinated sphere of each Zn²⁺ ion is completed by two carboxylate O atoms and two pyridine N atoms, well balancing the stability requirements from the hard and soft acid and base rule. On the other hand, the ultra-microporous cages and dual interpenetration of SNNU-334–336 greatly improve their structural stability. Overall, such a super thermal and chemical stability makes SNNU-334–336 MOFs promising gas adsorbents for possible industrial applications.

Gas uptake performance

Considering the accessible cage volume and high stability, the porosity of SNNU-334–336 was investigated by CO₂ adsorption at 195 K. It was found that the saturated adsorption capacity of SNNU-334–336 was 110 cm³ g⁻¹, 110 cm³ g⁻¹ and 120 cm³ g⁻¹, respectively (Fig. 2 and S3–S5†). The corresponding BET surface area was calculated to be 443.4 m² g⁻¹, 454.9 m² g⁻¹ and 489.6 m² g⁻¹, which are consistent with the increasing porosity from SNNU-334, SNNU-335 to SNNU-336 calculated by PLATON software (24.6%, 28.5% and 30.3%). The pore size distribution derived from the Horvath–Kawazoe model (Fig. 2d) demonstrates that the pore sizes of SNNU-334–336 are 0.34 nm, 0.34 nm, and 0.42 nm, indicating the existence of ultra-micropores in these MOF materials. Notably, the experimental pore sizes are slightly smaller than the diameters of cage A as a result of their dual interpenetration structures. Significantly, the reduced pore size is well comparable to the molecular sizes of C₂H₂ and CO₂, which thus provides a critical opportunity to purify C₂H₂.

Single component CO₂ and C₂H₂ adsorption measurements were performed at different temperatures. As shown in Fig. 3, the CO₂ uptake amounts of SNNU-334–336 at 273 K and 1 bar are 85.1 cm³ g⁻¹, 78.4 cm³ g⁻¹ and 92.7 cm³ g⁻¹, which are better than those of many reported ultra-microporous MOFs under the same conditions, such as Mn(bdc)(dpe) (45.9 cm³ g⁻¹),³⁰ Cd-NP (60.0 cm³ g⁻¹),² and PMOF-1 (53.3 cm³ g⁻¹).⁴³ The C₂H₂ uptakes of SNNU-334–336 are 66.8 cm³ g⁻¹, 63.0 cm³ g⁻¹ and 65.3 cm³ g⁻¹ at 273 K, respectively. It is worth noting that the uptake values of SNNU-334–336 for CO₂ are obviously higher than that of C₂H₂, which confirms that these three MOFs have inverse adsorption ability for C₂H₂/CO₂ mixtures. In addition, the uptake difference for CO₂ and C₂H₂ is 18.3 cm³ g⁻¹, 15.4 cm³

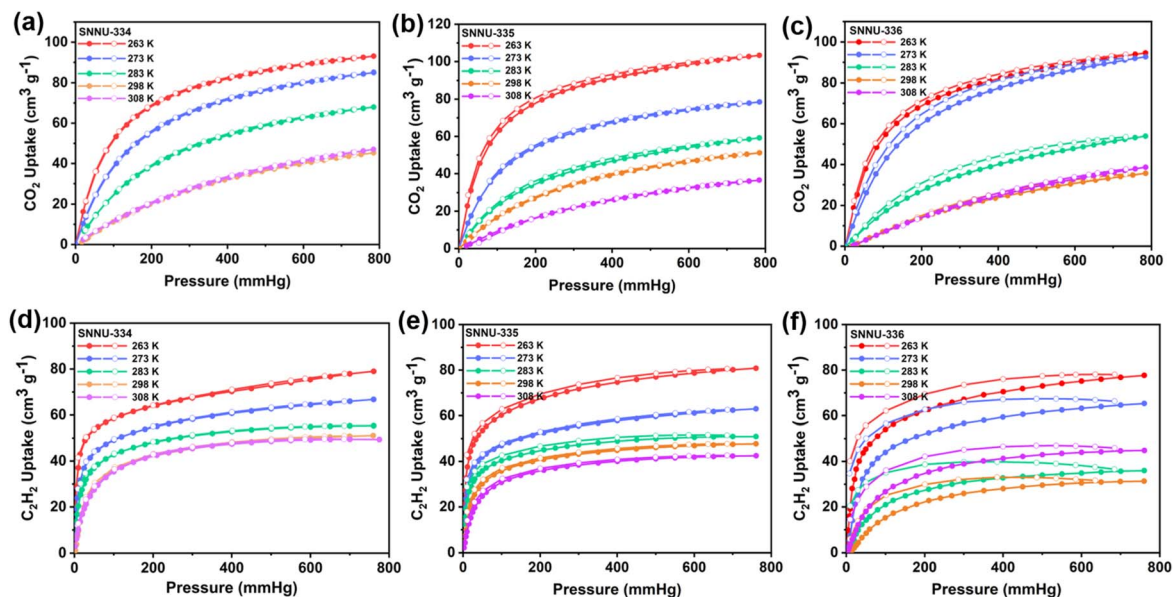


Fig. 3 The CO_2 (a, c and e) and C_2H_2 (b, d and f) adsorption isotherms of SNNU-334–336 at different temperatures.

g^{-1} , and $27.4 \text{ cm}^3 \text{ g}^{-1}$ for SNNU-334–336, which may indicate that SNNU-336 has the best inverse separation ability among the three MOFs.

As shown in Fig. S3b,† the adsorption curve of SNNU-334 at 273 K exhibits a fast increase for C_2H_2 uptake in the low-pressure region (<0.3 bar), while the increase for CO_2 adsorption is obviously slow with increasing pressure, indicating a stronger affinity of the MOF skeleton to C_2H_2 than CO_2 . When the pressure is further increased, both C_2H_2 and CO_2 gas uptakes increase more and more slowly, but the CO_2 adsorption capacity is higher than that of C_2H_2 in the high pressure region (Fig. S3b†), indicating an uncommon $\text{CO}_2/\text{C}_2\text{H}_2$ inverse adsorption behaviour. The intersection of the adsorption isotherms of C_2H_2 and CO_2 is named as the inverse pressure point. Interestingly, the adsorption behaviours of SNNU-334 change with the increase of temperature. The inverse points

gradually move to the high-pressure region from 263 K to 283 K (Fig. 4a). When the temperature reaches 298 K, the adsorption isotherms of C_2H_2 are always above that of CO_2 within the measured pressure region, but the trend is indicative of the possible reverse pressure point higher than 1 atm.

SNNU-335–336 MOFs demonstrate similar adsorption behaviours (Fig. 4b and c). Nevertheless, the adsorption behavior of SNNU-336 under the low-pressure region appears not as prominent as that for SNNU-334 and 335, as indicated by the smaller difference in the gas uptake of CO_2 and C_2H_2 in SNNU-336. This reveals that functionalization in TPB and BTC ligands has an important influence on the gas adsorption. It is noteworthy that the inverse adsorption can be regulated *via* the temperature in SNNU-334–336, as indicated by the temperature-dependent inverse pressure points (Fig. 4d). Such a phenomenon hasn't been observed for other reported MOF adsorbents until now. In other words, we can control the transition of SNNU-334–336 from CO_2 -selective MOFs to C_2H_2 -selective MOFs by adjusting the temperature.

The calculated Q_{st} values of C_2H_2 (38.3 kJ mol^{-1} for SNNU-334; $44.23 \text{ kJ mol}^{-1}$ for SNNU-335) are much higher than those of CO_2 (20.2 kJ mol^{-1} for SNNU-334; $38.07 \text{ kJ mol}^{-1}$ for SNNU-335) at low pressure (Fig. 5a and S6†). However, for SNNU-336 the Q_{st} value for C_2H_2 (48.7 kJ mol^{-1}) is similar to that of CO_2 (50.9 kJ mol^{-1}). This is indicative of the critical influence of functional groups on the interactions between active sites and different gas molecules. The largest Q_{st} difference of SNNU-334 in the three MOFs suggests that the central pyridyl group may have key effects on CO_2 and C_2H_2 adsorption.

According to the $\text{CO}_2/\text{C}_2\text{H}_2$ separation potential displayed by the adsorption isotherms, the $\text{CO}_2/\text{C}_2\text{H}_2$ separation performances of SNNU-334–336 were evaluated by using the ideal adsorption solution theory (IAST) (Fig. 5 and S7–S12†). The calculated IAST selectivity value of SNNU-334 at 273 K after the reverse point was 3595.4 at 1 atm ($\text{CO}_2/\text{C}_2\text{H}_2 = 50/50$). Under the

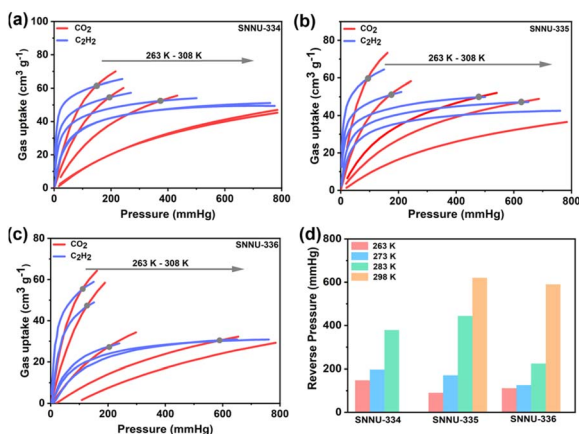


Fig. 4 The reversal points in C_2H_2 and CO_2 uptake isotherms for SNNU-334 (a), SNNU-335 (b) and SNNU-336 (c) at different temperatures, and a summary of the reverse pressure (d).

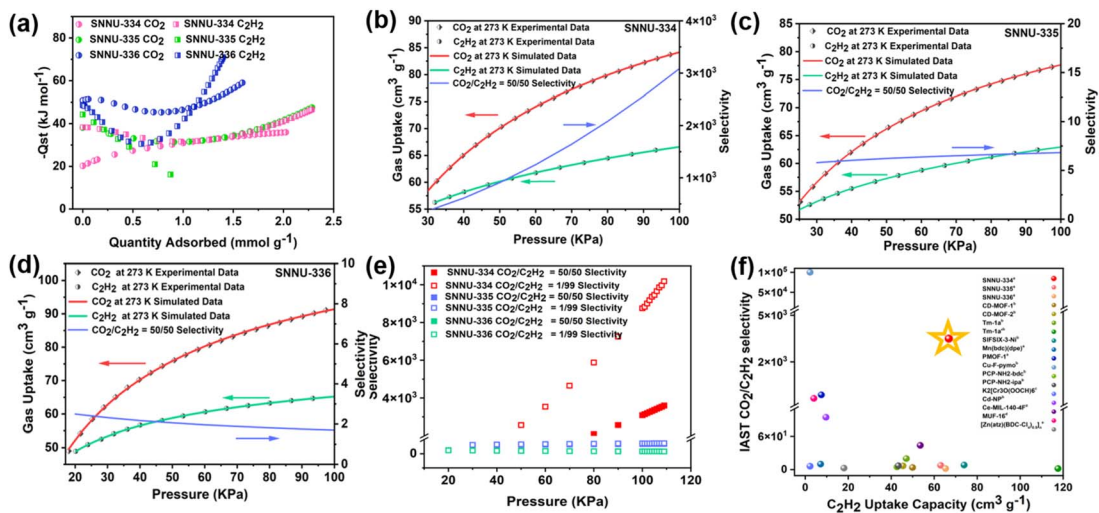


Fig. 5 (a) The calculated Q_{st} values for SNNU-334–336; (b–d) the IAST selectivity data calculated with a $\text{CO}_2/\text{C}_2\text{H}_2$ ratio of 50/50 after the reverse points at 273 K; (e) summary of IAST selectivity values with different $\text{CO}_2/\text{C}_2\text{H}_2$ ratios for SNNU-334–336 at 273 K (noted: $\text{CO}_2/\text{C}_2\text{H}_2$ (1/99) and $\text{CO}_2/\text{C}_2\text{H}_2$ (50/50) selectivity for SNNU-335 and SNNU-336 are very close with a difference within 0.5); (f) comparison of $\text{CO}_2/\text{C}_2\text{H}_2$ separation selectivity and C_2H_2 adsorption capacity of SNNU-334–336 with literature reported inverse $\text{C}_2\text{H}_2/\text{CO}_2$ separation MOF adsorbent materials (a-273 K, b-298 K, c-278 K, d-293 K and e-285 K).

same conditions, this value surpasses those of nearly all MOF materials with inverse $\text{C}_2\text{H}_2/\text{CO}_2$ separation performance, such as PMOF-1 (694),³³ MUF-16 (510),²⁵ Ce-MIL-140-4F (40),²⁴ and Mn(bdc)(dpe) (9.0).²³ At present, the selectivity is only lower than that of Cu-F-Pymo ($>10^5$), but the SNNU-334 material has a much higher adsorption capacity for CO_2 (Fig. 5f and Table S3†). When the ratio of $\text{CO}_2/\text{C}_2\text{H}_2$ becomes 1/99, the selectivity values calculated by IAST increase to 10 186.4 (Fig. S7c†). The calculated CO_2 over C_2H_2 IAST selectivity values for SNNU-335-

336 also well supports their adsorption results (Fig. S7–S12†) but are remarkably lower than that of SNNU-334, indicating that the decorated functional groups have a clear influence on the $\text{CO}_2/\text{C}_2\text{H}_2$ separation performance.

Dynamic breakthrough experiments

The prominent IAST selectivity data suggest the great potential of SNNU-334–336 for the practical separation of the $\text{CO}_2/\text{C}_2\text{H}_2$

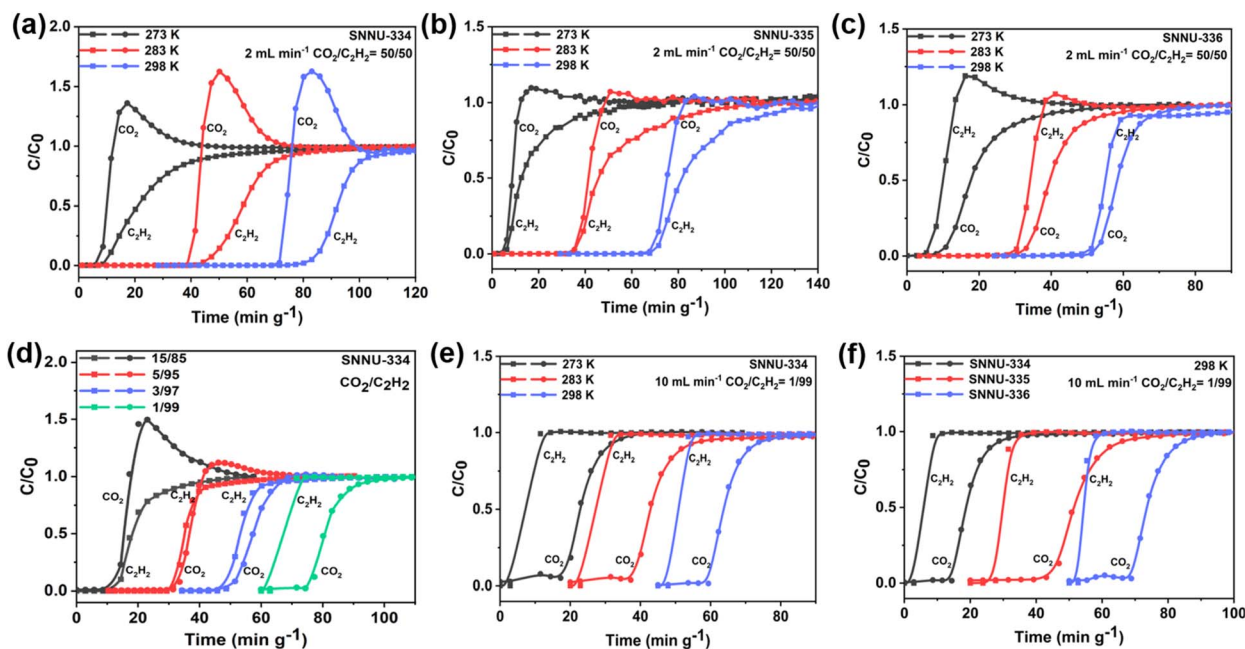


Fig. 6 Experimental breakthrough curves: $\text{CO}_2/\text{C}_2\text{H}_2 = 50/50$ for SNNU-334 (a), SNNU-335 (b), SNNU-336 (c) at different temperatures; different ratios of $\text{CO}_2/\text{C}_2\text{H}_2$ for SNNU-334 at 263 K (d), $\text{CO}_2/\text{C}_2\text{H}_2 = 1/99$ for SNNU-334 at different temperatures (e), and $\text{CO}_2/\text{C}_2\text{H}_2 = 1/99$ at 298 K of SNNU-334–336 (f).

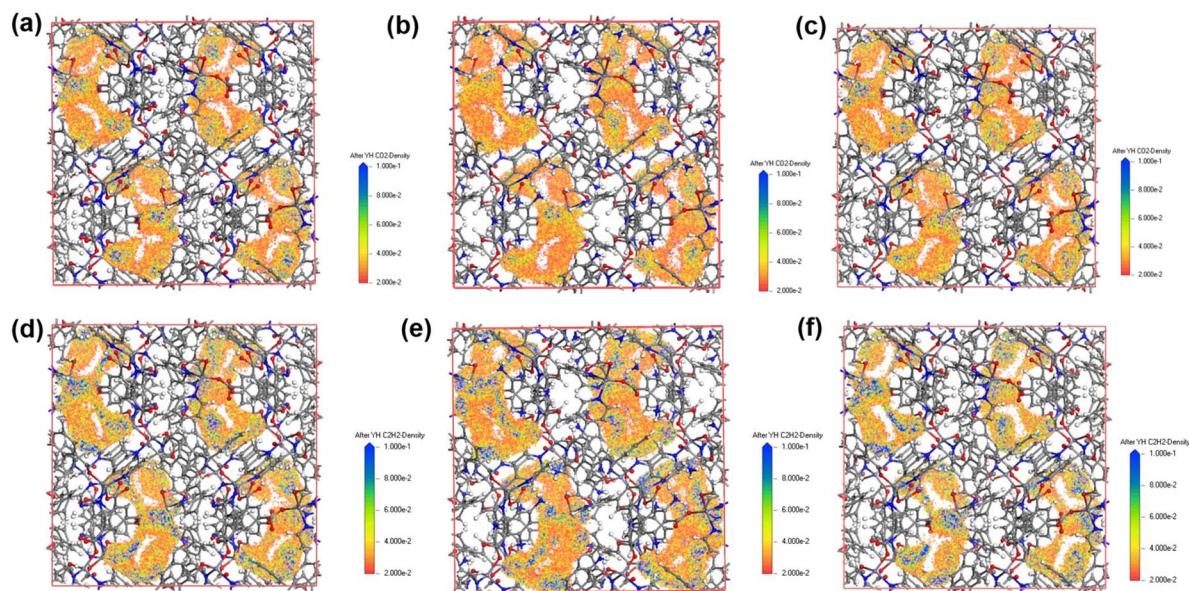


Fig. 7 GCMC simulation for density distributions of CO₂ and C₂H₂ at 298 K for SNNU-334 (a and d), SNNU-335 (b and e) and SNNU-336 (c and f).

mixture. Firstly, an equal molar CO₂/C₂H₂ mixture was tested as usual. The reverse separation of CO₂/C₂H₂ was not achieved by SNNU-334 and SNNU-335 at different temperatures, and the separation performance of SNNU-334 was better than that of SNNU-335 (Fig. 6 and S13–S17†). On the other hand, an inverse separation phenomenon is observed for SNNU-336. C₂H₂ molecules were detected first when equimolar CO₂/C₂H₂ mixtures were used although the separation ability was not outstanding. The completely different breakthrough results further indicate that functional groups have important influence on the separation of CO₂/C₂H₂ since their pore size is very close. SNNU-334–336 MOFs all are ultra-microporous structures, and the functional groups on the cage surface will have a great impact on the interactions between gas molecules and the MOF skeleton. In our opinion, the cage surface of SNNU-336 without any functional groups is more positive than that of SNNU-334 with pyridine or SNNU-335 with amino groups. Since the quadrupole moment of C₂H₂ is positive but CO₂ is negative, the repulsive force for C₂H₂ and attractive force for CO₂ both are largest in SNNU-336 among the three isostructural MOFs, thus resulting in an inverse separation process.

Furthermore, the separation of CO₂/C₂H₂ with different ratios was investigated. As shown in Fig. 6d, when the ratio of C₂H₂ gradually increased, SNNU-334 changed from preferentially detecting CO₂ to C₂H₂. When the CO₂/C₂H₂ ratio changed to 1/99, C₂H₂ was first detected at different temperatures, which was achieved in one-step to obtain C₂H₂ with a purity of more than 99.9% (Fig. 6e). Breakthrough experiments on SNNU-335 and SNNU-336 were also carried out under the same conditions (Fig. 6f), and the results indicated that SNNU-335–336 also performed well in directly obtaining high purity C₂H₂. Notably, 1.27 mmol g⁻¹ of C₂H₂ for SNNU-334, 1.70 mmol g⁻¹ of C₂H₂ for SNNU-335 and 1.19 mmol g⁻¹ of C₂H₂ for SNNU-336 with a purity of more than 99.9% were obtained. Such remarkable

productivity together with ultra-high purity indicates that SNNU-334–336 MOFs are potential adsorbents to efficiently remove trace CO₂ from acetylene *via* a one-step separation process.

GCMC simulation

To further understand the above CO₂/C₂H₂ adsorption and separation performance, GCMC simulations were performed to obtain the adsorption sites and density distributions of C₂H₂ and CO₂ molecules. The calculation results reveal that both C₂H₂ and CO₂ molecules are mainly distributed in cage A since cages B, C and D are blocked after the double interpenetration (Fig. 7). The load density of CO₂ in SNNU-335 was lowest (Fig. 7b), which is due to the presence of –NH₂ in SNNU-335 leading to the increasing steric hindrance effect which hinders the entry of gas molecules to a certain extent. When just one molecule of CO₂ or C₂H₂ was loaded into the skeleton of SNNU-336, as shown in Fig. S18e and f,† C₂H₂ molecules could form a C–H...N hydrogen bond (3.604 Å) with pyridine N atoms on the cage wall, and simultaneously interact with the benzene ring in the carboxylic acid ligand *via* C–H...π. In SNNU-334, due to the pyridine N in ligand TPP, the C–H...N hydrogen bond is stronger than that in SNNU-336, resulting in steeper adsorption curves for C₂H₂ in the low-pressure region (Fig. S18†). In SNNU-335, the steric effect of –NH₂ causes the C₂H₂ molecule to be no longer in the middle of the cage, but closer to the pyridine N. The C–H...N hydrogen bond is stronger than SNNU-336, resulting in steeper adsorption curves for C₂H₂ in the low-pressure region (Fig. S18†). On the other hand, CO₂ underwent C_{CO₂...O} and O_{CO₂...C} electrostatic interaction with uncoordinated carboxylic O and C (C_{CO₂...O} = 3.743–3.749 Å and O_{CO₂...C} = 3.661 Å) and acid–base interaction or electrostatic interaction. Multi-point contact may ultimately enhance the

interactions between CO₂ and the MOF skeleton, and thus lead to the inverse C₂H₂/CO₂ separation.

Conclusions

In summary, three new Zn-MOFs (SNNU-334–336) with different functional groups were successfully synthesized and demonstrated special inverse adsorption separation of CO₂/C₂H₂. The ultra-microporosity and dual interpenetrating structures enable these Zn-MOFs with unprecedented physical and chemical stability, which even can maintain their metal–organic skeleton integrity in boiling water. All Zn-MOFs exhibit unique CO₂ and C₂H₂ adsorption behaviours with the uptake reverse pressure points gradually moving towards high pressure with the increase of temperature. Besides extra-high CO₂ over C₂H₂ IAST selectivity, 99.9% purity of C₂H₂ can be obtained directly from the gas mixture containing CO₂ impurities with an intake CO₂/C₂H₂ ratio of 1/99. Overall, taking the extra-high framework stability, inverse adsorption separation ability, remarkable productivity, and extra-high purity into account, SNNU-334–336 materials may provide an ideal adsorbent platform to efficiently remove trace CO₂ from acetylene to produce highly pure C₂H₂ for industrial applications.

Author contributions

The authors declare no competing financial interest.

Conflicts of interest

There are no conflicts to declare.

Acknowledgements

This work was financially supported by the National Natural Science Foundation of China (22071140), the Natural Science Foundation of Shaanxi Province (2021JLM-20), and the Fundamental Research Funds for the Central Universities (GK202101002).

Notes and references

- 1 Y. P. Li, Y. Wang, Y. Y. Xue, H. P. Li, Q. G. Zhai, S. N. Li, Y. C. Jiang, M. C. Hu and X. Bu, *Angew. Chem., Int. Ed.*, 2019, **58**, 13590–13595.
- 2 Y. Xie, H. Cui, H. Wu, R. B. Lin, W. Zhou and B. Chen, *Angew. Chem., Int. Ed.*, 2021, **60**, 9604–9609.
- 3 Q. Dong, Y. Guo, H. Cao, S. Wang, R. Matsuda and J. Duan, *ACS Appl. Mater. Interfaces*, 2020, **12**, 3764–3772.
- 4 K.-J. Chen, H. S. Scott, D. G. Madden, T. Pham, A. Kumar, A. Bajpai, M. Lusi, K. A. Forrest, B. Space, J. J. Perry and M. J. Zaworotko, *Chem*, 2016, **1**, 753–765.
- 5 S. Mukherjee, Y. He, D. Franz, S. Q. Wang, W. R. Xian, A. A. Bezrukov, B. Space, Z. Xu, J. He and M. J. Zaworotko, *Chemistry*, 2020, **26**, 4923–4929.
- 6 R. Matsuda, R. Kitaura, S. Kitagawa, Y. Kubota, R. V. Belosludov, T. C. Kobayashi, H. Sakamoto, T. Chiba, M. Takata, Y. Kawazoe and Y. Mita, *Nature*, 2005, **436**, 238–241.
- 7 W. Fan, S. Yuan, W. Wang, L. Feng, X. Liu, X. Zhang, X. Wang, Z. Kang, F. Dai, D. Yuan, D. Sun and H.-C. Zhou, *J. Am. Chem. Soc.*, 2020, **142**, 8728–8737.
- 8 Y. Shi, Y. Xie, H. Cui, Y. Ye, H. Wu, W. Zhou, H. Arman, R. B. Lin and B. Chen, *Adv. Mater.*, 2021, **33**, e2105880.
- 9 R. Liu, Q. Y. Liu, R. Krishna, W. Wang, C. T. He and Y. L. Wang, *Inorg. Chem.*, 2019, **58**, 5089–5095.
- 10 C. R. Reid and K. M. Thomas, *J. Phys. Chem. B*, 2001, **105**, 10619–10629.
- 11 Y. Zhang, J. Hu, R. Krishna, L. Wang, L. Yang, X. Cui, S. Duttwyler and H. Xing, *Angew. Chem., Int. Ed.*, 2020, **59**, 17664–17669.
- 12 R.-B. Lin, L. Li, H. Wu, H. Arman, B. Li, R.-G. Lin, W. Zhou and B. Chen, *J. Am. Chem. Soc.*, 2017, **139**, 8022–8028.
- 13 B. S. Gelfand, R. P. S. Huynh, R. K. Mah and G. K. H. Shimizu, *Angew. Chem., Int. Ed.*, 2016, **55**, 14614–14617.
- 14 F. Moreau, I. da Silva, N. H. Al Smail, T. L. Easun, M. Savage, H. G. W. Godfrey, S. F. Parker, P. Manuel, S. Yang and M. Schröder, *Nat. Commun.*, 2017, **8**, 14085.
- 15 W. Fan, X. Wang, X. Liu, B. Xu, X. Zhang, W. Wang, X. Wang, Y. Wang, F. Dai, D. Yuan and D. Sun, *ACS Sustainable Chem. Eng.*, 2018, **7**, 2134–2140.
- 16 D. Luo, X.-P. Zhou and D. Li, *Angew. Chem., Int. Ed.*, 2015, **54**, 6190–6195.
- 17 J. Pei, J.-X. Wang, K. Shao, Y. Yang, Y. Cui, H. Wu, W. Zhou, B. Li and G. Qian, *J. Mater. Chem. A*, 2020, **8**, 3613–3620.
- 18 H. Cai, M. Li, X.-R. Lin, W. Chen, G.-H. Chen, X.-C. Huang and D. Li, *Angew. Chem., Int. Ed.*, 2015, **54**, 10454–10459.
- 19 H. Jiang, D. Alezi and M. Eddaoudi, *Nat. Rev. Mater.*, 2021, **6**, 466–487.
- 20 Y. Belmabkhout, V. Guillerm and M. Eddaoudi, *Chem. Eng. J.*, 2016, **296**, 386–397.
- 21 X.-P. Fu, Y.-L. Wang, X.-F. Zhang, Z. Zhang, C.-T. He and Q.-Y. Liu, *CCS Chem.*, 2022, **4**, 3416–3425.
- 22 X.-P. Fu, Y.-L. Wang, X.-F. Zhang, R. Krishna, C.-T. He, Q.-Y. Liu and B. Chen, *Chem. Eng. J.*, 2022, **432**, 134433–134440.
- 23 X. P. Fu, Y. L. Wang and Q. Y. Liu, *Dalton Trans.*, 2020, **49**, 16598–16607.
- 24 J. Lee, C. Y. Chuah, J. Kim, Y. Kim, N. Ko, Y. Seo, K. Kim, T. H. Bae and E. Lee, *Angew. Chem., Int. Ed.*, 2018, **57**, 7869–7873.
- 25 M. Jiang, X. Cui, L. Yang, Q. Yang, Z. Zhang, Y. Yang and H. Xing, *Chem. Eng. J.*, 2018, **352**, 803–810.
- 26 X.-J. Kong, Y.-Z. Zhang, T. He, X.-Q. Wu, M.-M. Xu, S.-N. Wang, L.-H. Xie and J.-R. Li, *CrystEngComm*, 2018, **20**, 6018–6025.
- 27 R. Eguchi, S. Uchida and N. Mizuno, *Angew. Chem., Int. Ed.*, 2012, **51**, 1635–1639.
- 28 W. Yang, A. J. Davies, X. Lin, M. Suyetin, R. Matsuda, A. J. Blake, C. Wilson, W. Lewis, J. E. Parker, C. C. Tang, M. W. George, P. Hubberstey, S. Kitagawa, H. Sakamoto, E. Bichoutskaia, N. R. Champness, S. Yang and M. Schröder, *Chem. Sci.*, 2012, **3**, 2993–2999.

- 1 29 S.-Q. Yang and T.-L. Hu, *Coord. Chem. Rev.*, 2022, **468**, 214628. 1
- 30 M. L. Foo, R. Matsuda, Y. Hijikata, R. Krishna, H. Sato, S. Horike, A. Hori, J. Duan, Y. Sato, Y. Kubota, M. Takata and S. Kitagawa, *J. Am. Chem. Soc.*, 2016, **138**, 3022–3030. 5
- 31 Z. Zhang, S. B. Peh, R. Krishna, C. Kang, K. Chai, Y. Wang, D. Shi and D. Zhao, *Angew. Chem., Int. Ed.*, 2021, **60**, 17198–17204.
- 32 O. T. Qazvini, R. Babarao and S. G. Telfer, *Nat. Commun.*, 2021, **12**, 197. 10
- 33 L. Li, J. Wang, Z. Zhang, Q. Yang, Y. Yang, B. Su, Z. Bao and Q. Ren, *ACS Appl. Mater. Interfaces*, 2019, **11**, 2543–2550.
- 34 D. Ma, Z. Li, J. Zhu, Y. Zhou, L. Chen, X. Mai, M. Liufu, Y. Wu and Y. Li, *J. Mater. Chem. A*, 2020, **8**, 11933–11937.
- 15 35 X.-Y. Li, Y. Song, C.-X. Zhang, C.-X. Zhao and C. He, *Sep. Purif. Technol.*, 2021, **279**, 119608.
- 36 X. C. Huang, Y. Y. Lin, J. P. Zhang and X. M. Chen, *Angew. Chem., Int. Ed.*, 2006, **45**, 1557–1559. 20
- 37 M. Ding, X. Cai and H. L. Jiang, *Chem. Sci.*, 2019, **10**, 10209–10230. 1
- 38 Z. N. Kyo Sung Park, A. P. Côté, J. Y. Choi, R. Huang, F. J. Uribe-Romo, H. K. Chae and O. M. Y. Michael O’Keeffe, *Proc. Natl. Acad. Sci. U. S. A.*, 2006, **103**, 10186–10191. 5
- 39 X. Liu, N. K. Demir, Z. Wu and K. Li, *J. Am. Chem. Soc.*, 2015, **137**, 6999–7002.
- 40 O. V. Dolomanov, L. J. Bourhis, R. J. Gildea, J. A. K. Howard and H. Puschmann, *J. Appl. Crystallogr.*, 2009, **42**, 339–341. 10
- 41 G. Sheldrick, *Acta Crystallogr., Sect. A: Found. Adv.*, 2014, **70**, C1437.
- 42 G. Sheldrick, *Acta Crystallogr., Sect. A: Found. Crystallogr.*, 2008, **64**, 112–122.
- 15 43 L. Z. Cai, Z. Z. Yao, S. J. Lin, M. S. Wang and G. C. Guo, *Angew. Chem., Int. Ed.*, 2021, **60**, 18223–18230. 15
- 20 20
- 25 25
- 30 30
- 35 35
- 40 40
- 45 45
- 50 50
- 55 55